Long-Term Characterization of Firing Dynamics of Spontaneous Bursts in Cultured Neural Networks

Jaap van Pelt*, Pieter S. Wolters, Michael A. Corner, Wim L. C. Rutten, *Member, IEEE*, and Ger J. A. Ramakers

Abstract—Extracellular action potentials were recorded from developing dissociated rat neocortical networks continuously for up to 49 days *in vitro* using planar multielectrode arrays. Spontaneous neuronal activity emerged toward the end of the first week *in vitro* and from then on exhibited periods of elevated firing rates, lasting for a few days up to weeks, which were largely uncorrelated among different recording sites. On a time scale of seconds to minutes, network activity typically displayed an ongoing repetition of distinctive firing patterns, including short episodes of synchronous firing at many sites (*network bursts*). Network bursts were highly variable in their individual spatio-temporal firing patterns but showed a remarkably stable underlying probabilistic structure (obtained by summing consecutive bursts) on a time scale of hours. On still longer time scales, network bursts evolved gradually, with a significant broadening (to about 2 s) in the third week *in vitro*, followed by a drastic shortening after about one month *in vitro*. Bursts at this age were characterized by highly synchronized onsets reaching peak firing levels within less than ca. 60 ms. This pattern persisted for the rest of the culture period. Throughout the recording period, active sites showed highly persistent temporal relationships within network bursts. These longitudinal recordings of network firing have, thus, brought to light a reproducible pattern of complex changes in spontaneous firing dynamics of bursts during the development of isolated cortical neurons into synaptically interconnected networks.

Index Terms—Cell culture, neuronal network development, rat cerebral cortex, spike-train analysis, spontaneous bursting patterns.

I. INTRODUCTION

DURING early development of the central nervous system (CNS), nerve cells form extensive interconnections, thereby creating functional neuronal networks exhibiting frequent spontaneous action potential discharges, see [1]–[4]. Conversely, cellular processes involved in network connectivity are themselves modulated by bioelectric activity (e.g., [5]–[12]). A reciprocal influence, thus, exists between the development of neuronal connectivity on the one hand, and intrinsic bioelectric network activity on the other hand (see [2]

*J. van Pelt is with the Graduate School Neurosciences Amsterdam, Netherlands Institute for Brain Research, Neurons and Networks Research Group, 1105 AZ Amsterdam, The Netherlands (e-mail: j.van.pelt@nih.knaw.nl).

P. S. Wolters, M. A. Corner, and G. J. A. Ramakers are with the Graduate School Neurosciences Amsterdam, Netherlands Institute for Brain Research, Neurons and Networks Research Group, 1105 AZ Amsterdam, The Netherlands.

W. L. C. Rutten is with the Biomedical Signals and Systems Department/Faculty of Electrical Engineering/Institute for Biomedical Technology, University of Twente, 7500 AE Enschede, The Netherlands.

and [13]–[16]). The degree to which structure and function in different CNS structures are determined by this reciprocal relationship is still far from resolved. Especially the role of spontaneous bioelectric activity (SBA), which initially constitutes the major portion of the ongoing functional interactions in developing networks (reviewed by [2]), has not yet been approached in a comprehensive manner.

Most of the evidence for activity-dependent processes governing neurite outgrowth has been obtained either from isolated neurons or from population-based experiments under defined conditions of either bioelectric activity (e.g., [17]–[19]) or intracellular calcium levels (e.g., [11]; [20], [21]). According to a hypothesis originally formulated by [20], maximal outgrowth will take place at an optimal intracellular calcium level; otherwise outgrowth will be retarded or even reversed. By modulating intracellular calcium levels, variations in activity levels could, thus, contribute to the morphological variance among neurons. Recent time-lapse studies have indeed demonstrated a rapid formation of lamellipodia and subsequent long-lasting increases in branching following experimental depolarization of cultured rat cerebral cortex neurons [18].

Not only the morphology, however, but also the physiology of neocortical tissue developing *in vitro* is sensitive to variations in the level and/or patterning of SBA, so that spontaneous spike trains themselves reflect the functional electrophysiological history of the network during its formative period [2]. To study how such activity shapes the mature morphology of individual neurons, one would need to know the cumulative "experience" of each neuron in terms of the levels and patterns of its discharges at different developmental stages. Such experiments would ideally be coupled to investigations in which the firing activity profile is either correlated with cytomorphological information at selected time points or, better still, monitored in parallel with ongoing structural measurements. Correlation analysis would then address the question of whether activity-dependent mechanisms appear to link the morphological development of identified neurons with aspects of their electrophysiological history.

As a first step toward realizing such an experimental paradigm, we have studied the spontaneous firing activity of many neurons simultaneously and continuously during their development into a synaptically connected network. Rodent neocortical neurons (see [22]) were cultured on multielectrode plates (MEPs) [23] enabling continuous monitoring of SBA from up to 60 sites over a period of several weeks. Such cultures display spontaneous bioelectric activity already in an early phase of network formation, often in patterns closely approximating those seen *in vivo* (see [2]). The pioneering work of Gross (e.g., [24]; [25]) and of Pine [26] has evolved to the point where, as recently shown by [27], long-term multielectrode registration
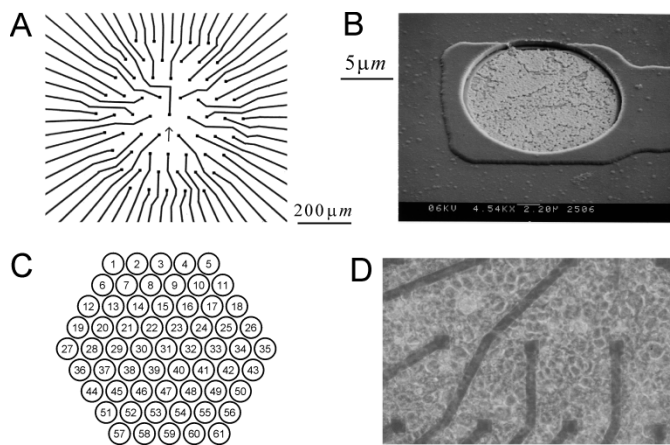
Fig. 1. (a) Inner area of an MEP showing the electrically conductive leads ending in a hexagonal pattern of electrode tips. The leads are 10 μm in width and the tips have a mutual distance of 70 μm. (b) SEM image illustrating the geometry of an electrode tip and the de-insulated area with a diameter of 12 μm. The insulation layer is composed of an 800-nm-thick sandwich of SiO_2, Si_3N_4, and SiO_2 (ONO, from oxide, nitride, oxide). The electrode tip in the image is electroplated with platinum. (c) Numbering of the 61 electrode tips. (d) Inner area of a dissociated rat cortex tissue culture on an MEP showing a confluent monolayer of cells.

can be utilized for the study of activity-dependent plasticity at the synaptic level. In the present paper, we report the continuous longitudinal recording of neuronal spike discharges during neocortical network development over a period of 4–7 weeks *in vitro* (WIV). The results have brought to light hitherto unknown properties of spontaneous firing dynamics in these networks, such as long-lasting transient periods of increased firing at individual sites on a time scale of days to weeks and an age-specific repetitive pattern of coordinated network firing on a time scale of seconds. Especially the spatio-temporal organization of firing within network bursts showed great stability over many hours. In addition, a progressive day-to-day evolution was observed, with an initial broadening of the burst envelope during the third WIV and a pattern of abrupt onset and precise spike timing from the fifth WIV onwards. Preliminary reports of the data have previously appeared in [23].

II. MATERIALS AND METHODS

A. MEP Design

MEPs were obtained from the University of Twente, Enschede, The Netherlands (see [28]). The MEPs consist of 5×5 cm glass plates onto which a pattern of 61 electrically conductive lanes (indium–tin–oxide or gold) was deposited, running from two sides of the plate toward a central area where they ended in a hexagonal pattern of electrodes with a diameter of 12 μm, spaced 70 μm apart (Fig. 1) a pattern similar to the layout used by [29].

B. Production of MEPs and Culture Chambers

MEPs were produced with either transparent indium–tin–oxide (ITO: see [30]) or with gold as the electrically conductive medium (ITO glass plates were obtained from Philips, Heerlen, The Netherlands). The electrode pattern on the ITO glass plates was etched from the ITO layer using positive photoresist photo-lithographic techniques. On glass

plates containing a 100-nm-thick layer of ITO, a layer of Microposit S1818 photoresist (Microposit, Coventry, U.K.) was spun and cured for 20 min at 90 °C. The photoresist was illuminated through a mask and developed with Microposit S1813 (Microposit). The developed photoresist was etched for 9 min at 45 °C with a HCl–H_2O–HNO_3, (50:50:1, v/v/v) solution. Subsequently, the MEPs were covered with an insulation layer consisting of a *sandwich* of SiO_2, Si_3N_4, and SiO_2, i.e., silicon oxide, silicon nitride, and silicon oxide layers (ONO, total thickness $\leq$ 800 nm). These layers were created by plasma-enhanced chemical vapor deposition (PECVD). The silicon oxide layers were deposited for 3 min under gaseous SiH_4, 2% N_2, and N_2O conditions. The silicon nitride layer was deposited for 36 min under gaseous SiH_4, 2% N_2, and NH_3 conditions. Finally, the electrode tips were de-insulated (diameter 12 μm) using reactive ion etching (RIE) with gaseous SF_6 and O_2 for 6 min [Fig. 1(d)] and then platinized in order to reduce their impedance (resistive part) to less than 1 MΩ at 1 kHz [31].

The electrode lanes and sites on the gold glass plates were made by gold deposition, with a layer thickness of 100 nm. For better adhesion to the glass and the next ONO (SiO_2-Si_3N_4-SiO_2 sandwich) layer, a 10-nm titanium layer was applied under and on top of the gold layer. The superfluous gold and titanium layers were etched away with an RIE process, using a plasma of O_2 and CHF_3.

Besides electrode impedance, the sealing resistance is an important parameter in recording activity from a cell [31], [32]. Good sealing prevents current leakage from the gap between cell and electrode (or surrounding substrate) into the medium. The sealing resistance in our setup was estimated at circa 5 MΩ [31].

A culture chamber was created by fixing a glass cylinder with an inner diameter of 30 mm onto the MEP, using silicone elastomere (Dow Corning 3140 RTV coating). MEPs were placed in a closed incubation chamber, mounted on an inverted microscope, and kept at a constant temperature of 36 °C in a 5% humidified CO_2 environment.

In addition, commercial multielectrode arrays, containing electrodes of different diameters (10, 20, and 30 μm (HEXA MEAs, Multi Channel Systems, Reutlingen, Germany), have been used in order to study the effect of electrode size on the number of units contributing to the spiking activity of the electrode.

C. Cell Cultures

The cortices of E18 Wistar rat fetuses were removed and dissociated by trituration following treatment with trypsin [18], [22]. The dissociated neurons were plated in a 7-mm round spot in the center of the MEP coated with polyethylene-imine (PEI, Fluka, 10 mg/ml) using glass rings (inner diameter of 7 mm). PEI is a synthetic basic polymer whose chemical and adhesive properties are similar to the more commonly used poly-lysine or poly-ornithine but which has the advantage that it is not biodegradable. As a result, adhesion of neurons is rapid and stable over a period of at least two months. Moreover, as indicated by phase contrast observations and immunocytochemical staining for axonal markers, PEI also prevents bundling of axons. More natural substrates, such as laminin or collagen, result in reasonable initial adhesion, but in these cases neurons

are initially able to migrate so as to become aggregated within a few days, whereafter the aggregates gradually become detached from the MEPs. A combination of PEI and laminin gives better long-term adhesion than does laminin alone, but neurons still aggregate after several weeks. In general, any condition that allows neurons to migrate even slightly, will result in their aggregation. This indirect indication that neurons are not able to migrate on PEI substrates was verified by time-lapse imaging. Whereas glial cells can migrate freely, neuronal cell bodies do not appear to move at all, at the optical resolution of a light microscope fitted with an objective of 63×1.4 n.a. ($<0.2~\mu$m). Neuronal growth cones, on the other hand, move around largely unhindered, giving rise to long axons and dendrites. Over the course of three weeks, axons can reach lengths of more than 10 mm (Ramakers, investigation in progress).

In total, 150 000 cells (50 μl cell suspension) were plated. After 1 h, the rings were removed, and 10^6 cells in 1 ml of cell suspension were added to the culture chamber on the MEP (inner diameter 30 mm). For the inner area, this resulted in a monolayer of cells in such a density that a surface area on the average of 200 μm^2 (corresponding to a 16 μm circle diameter) was available for each cell. At the time of plating, the cells themselves had a diameter of about 5 μm, which increased to about 15 μm by three weeks.

Neurons were cultured and recorded in 2 ml of glia conditioned medium (GCM) $+0.2\%$ BSA containing 1.3 mM Ca^{2+} and 0.7 mM Mg^{2+}. GCM was produced by incubating confluent glial cultures for four days in a serum-free, chemically defined medium (EMR). This resulted in conditioning of the EMR with glia-derived factors essential for long-term survival of the neurons. The EMR consisted of a mixture of 50% DMEM and 50% Ham's F12 medium from which glutamate and aspartate were deleted and to which the following essential components were added: insulin (bovine; 10 μg/ml; Sigma), apo-transferrin (human; 50 μg/ml), thioctic acid (0.25 μg/ml), tocopherol (10 μg/ml), retinol (1 μg/ml), biotin (10 μg/ml), sodium pyruvate (100 μg/ml; all from Sigma), and glutamax (2 mM; Gibco). EMR was purchased from Invitrogen/Gibco as a powdered "special" medium that was reconstituted with pyrogen-free medium, sterile-filtered, and further supplemented to obtain the final medium.

Glial cultures were produced by dissociating newborn rat cerebra (containing neocortex, hippocampus, and basal ganglia, but not the meninges) by mechanical dissociation and plating five million cells in 50 ml of DMEM with 10% fetal calf serum (D10) in a T175 tissue culture flask (Nunc). When the gial cells reached confluency (usually after 10–14 days), the D10 was taken off and rinsed with 5 ml ERM, after which 50 ml EMR was conditioned by the glia for four days.

The culture chambers were covered with a glass lid and firmly sealed with parafilm in order to prevent evaporation of the medium during the long-term recording period. Once a week, about 200 μl of the medium was replaced by 300 μl of fresh medium. No further handling was applied during the entire recording period. These culturing conditions (see, also, [33]) ensured stable osmolarity as well as pH levels, with fluctuations of the former staying within 3% or less over a period of 29 days *in vitro* (DIV). After each experiment, the MEPs were cleansed by careful rinsing and then sterilized for 4 h at 140 °C for reuse.
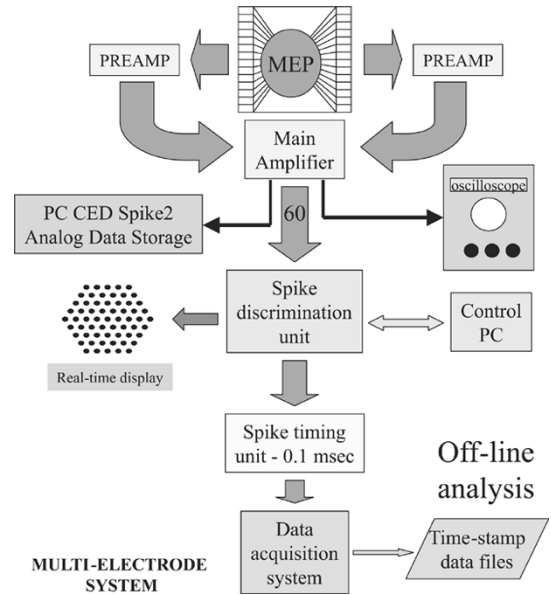

Fig. 2. Schematic representation of the multielectrode system. Culture assembly, preamplifiers, and connectors are placed in a temperature-controlled setup.

D. Multielectrode Recording Setup (Fig. 2)

Amplifiers: Two miniaturized 30-channel preamplifiers with an input impedance of 10 MΩ and $100 \times$ amplification were positioned on either side of the MEP and were connected to the tabs by means of zebra strips (Fujipoly, Kenilworth NJ). The signals were subsequently fed into an array of main amplifiers with $220 \times$ amplification (bandwidth: 250 Hz–5 kHz, -12 dB/octave). The input-equivalent noise level of the amplifiers was 3 μV

Electrode Noise Levels: Estimations for thermal noise levels can be obtained from the expression $E_{\mathrm{rms}} = \sqrt{4kTBR}$ for thermal noise E_{rms} in a resistor R at absolute temperature $T = 294$ K, with Boltzmann's constant $k = 1.380710^{-23}$ JK^{-1} and bandwidth $B = 5000 - 250 = 4750$ Hz. Thus, thermal noise over a resistance of 1 MΩ, for instance, would be expected to have an root mean squared (rms) value of about 9 μV.

Spike Discrimination Unit: The analog signals from the main amplifier were fed into a homemade 60-channel spike discrimination unit, constructed on the basis of programmable integrated circuit chips (PIC16C74A from Microchip). The signals were sampled at 22.2 kHz and spikes were identified when the signals crossed preset discriminator levels. Prior to each recording period, these levels were automatically and independently set for each channel at a factor 1.9 times the median of 11 positive maximum signal levels, measured in 11 successive 2-ms time bins at that channel. This procedure had been shown in pilot experiments to be a reliable and fast way for determining discriminator levels, which were checked to effectively discriminate against noise.

Time-Stamp Unit: The unitary pulses from the spike discrimination unit were fed into a time-stamp unit (built around a DIO-128 state-change monitoring system; Viewpoint Systems Inc., Rochester, NY) for accurate time marking at their leading edge (precision of 100 μs). The system was operated through

a homemade application developed using National Instruments LabVIEW software.

Analog Recordings: Parallel to the discrimination unit, the analog signals from the main amplifiers were also fed into a CED1401+ general purpose signal processing interface (Cambridge Electronic Design, Cambridge, U.K.). Routinely, prior to the start of a new run, short stretches of analog signals (10 frames of 400 ms for each active site, triggered by action potentials) were digitized and stored with CED Signal and Spike2 software. This enabled us to regularly monitor noise levels and shapes of action potentials during the experiment. During the experiment, noise levels were routinely displayed and observed on a storage oscilloscope (Tektronix, TDS 310, Wilsonville, OR).

Visual Display: The output of the spike discriminator unit was also made visible by means of an LED display with a layout geometrically similar to the MEP layout. The LED display proved to be very useful for online visualization of the spatio-temporal patterns of activity within the cultured network. The detected spikes were simultaneously monitored acoustically.

E. Experimental Protocol

For each E18 pregnant Wistar rat, an average number of seven cultures were prepared on as many MEPs from the cortices of its fetuses. From the end of the first WIV on, up to four cultures per day were screened for spontaneous activity, comprising half-hour accommodation of the culture in the recording setup and a subsequent period of 1 h for screening active sites. Once a culture was encountered which showed ongoing spontaneous activity on at least four sites, it was selected for a continuous longitudinal measurement and maintained in the recording setup (thus terminating the screening of the other MEPS). According to this experimental protocol, five cultures were obtained from which activity could be recorded for periods ranging from 30 DIV to 7 WIV.

F. Data Acquisition

Action potentials from 60 recording sites were collected in consecutive 100 μsec time bins and stored as "events," which were labeled with the clock time (running at 10 kHz) and the bit pattern indicating at which sites an action potential had occurred within that time bin. The longitudinal recording was briefly interrupted (typically less than one hour) at the end of each day (or weekend) in order to save these data files and to monitor noise levels and spike shapes, after which a new "run" was started. A complete longitudinal experiment, thus, consisted of a series of consecutive runs with the same culture, with each run lasting one or more days.

G. Data Processing

Detection of "Network Bursts": On a time-scale of seconds, spontaneous activity was seen to display a clearcut repetitive pattern, with the repetitive periods typically including a phase of sustained firing, a short phase of intense firing with recruitment of many active sites (network bursts), and a variable quiescent phase. The latter are identifiable in interspike interval histograms as a distinct peak at long intervals (usually 2–3 s or
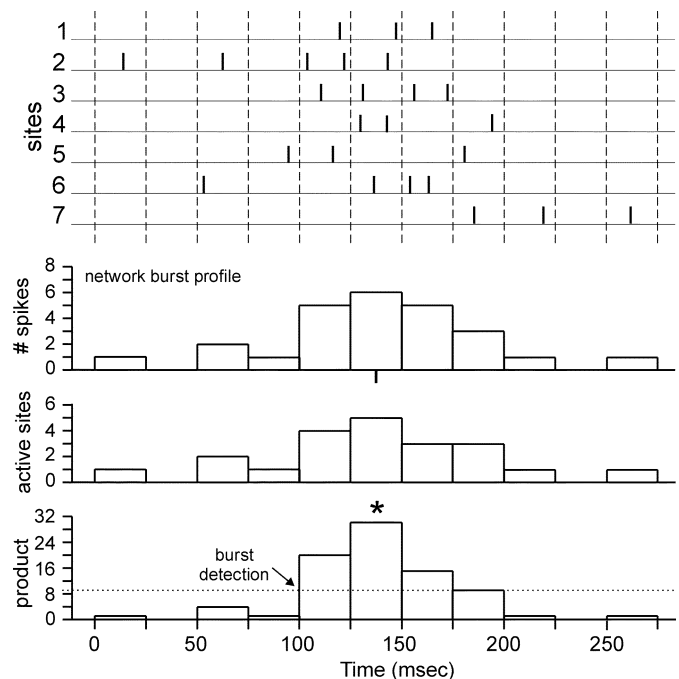

Fig. 3. Illustration of the procedure for burst detection. The upper part displays an arbitrary pattern of spikes at seven sites. The lower part displays the histograms for the number of spikes and the number of active sites, counted for a time division of 25 ms. The lowest panel displays the product of the spike count and the active-site count. A "burst" is considered to have been detected when this product exceeds the value 9, as indicated by the arrow. The time bin with the maximal product value (see star) is taken as the center of the burst, which is delineated by a small line underneath the spike count histogram (i.e., network burst profile).

more). Each repetitive period of firing, thus, includes a series of spikes with interspike time intervals smaller than the observed silent periods (spike cluster). By choosing an interspike time interval criterion value (see [2] and [34]) that separates these peaks of short and long intervals, the stream of network spikes could be automatically split up objectively into clusters of spikes of interspike time intervals smaller than the criterion, whose clusters closely correspond to the individual repetitive periods. A criterion value of 1.3 s for use in the present experiments was estimated by comparing the interspike time-interval histograms calculated in the course of each recording period. Each spike cluster was then scanned for the presence of network bursts, the most intense of which was then analyzed as follows.

Network bursts were automatically detected using the property that both the network firing rate and number of contributing sites become larger during such bursts. For network burst detection then, we calculated the product of the number of active sites and the total number of spikes at these sites, as evaluated using 25-ms time bins. This product was required to equal or exceed a chosen value of 9, a value that in practice was adequate to capture bursts throughout the entire recording period (see Fig. 3). The center of a burst was taken as the time point at which this product was maximal (indicated by a star in Fig. 3). For obtaining a value for the width of the burst, the "boundary" time points at which the firing rate had fallen to <5% of the peak value were first calculated on both sides of the center. Subsequently, the time points were calculated on the left and right sides that equally divide the total number of spikes between

the boundaries and the center, thus giving the half-width of the rising and falling phase of the burst, respectively. The half-width of the total burst was then taken to be the time interval between the two "50% time points."

Spatio-Temporal Structure of Firing Within Network Bursts: Since spatio-temporal patterns of firing among individual network bursts were highly variable, the underlying probabilistic structure was obtained by summation of a large number of consecutive bursts. Since, in contrast to stimulus-response experiments, there is no externally defined time mark for alignment in our recordings, we took the center of each network burst as the alignment time mark. Network bursts were then summed using time-bins of 10 ms over a window of 4 s centered on the alignment time mark. These values were chosen so as to obtain a finely resolved and statistically stable shape of network bursts. Action potentials were counted for each site in the appropriate time bins for all network bursts occurring during a continuous period of 4 h. The summed plot for each site, thus, shows its mean firing rate during network bursts as a function of time from onset to termination.

III. RESULTS

A. Spike Shapes and Noise Levels

Noise levels were typically at the order of 7-μV rms [see Fig. 4(b)], corresponding to the thermal noise generated over an impedance of 0.64 MΩ (see Section II). For such noise levels, the spike discrimination level was automatically set at ca. 19 μV. In all experiments, there were sites from which few or no action potentials were recorded during the entire recording period, indicating that the adopted method of spike discrimination was effective in excluding noise.

Spike amplitudes were not strictly constant over prolonged recording periods [Fig. 4(a) and (f)], but their fluctuations remained within a restricted amplitude range, with the lowest values considerably above the spike discrimination thresholds, as also illustrated by the mean amplitudes as well as the stable sd values in Fig. 4(f). One of the examples in Fig. 4(a) shows an initial increase in spike amplitude followed by a period with similar fluctuations as in the other examples. Visual inspection of spike shape and amplitude during the recording sessions revealed that approximately 50% of the active sites showed solely large monophasic negative action potentials [Fig. 4(b)]. In the other cases, spikes from more than one unit were clearly evident on the oscilloscope tracings, but one of them usually had such higher spike amplitude than the other(s), that a single (negative) voltage discrimination threshold was still effective in extracting only this unit for analysis. Single-unit detection was then confirmed on the basis of the interspike interval distributions, which consistently showed refractory periods of 2–3 ms [e.g., Fig. 4(c) and (d)].

All such extracted single units displayed the relatively broad waveform characteristic for cell somata [35] and contrasted sharply with the small fast (putative axon) spikes which were occasionally seen and heard but which did not contribute to the stored time stamps (as monitored on a storage oscilloscope). Recent unpublished experiments in which the cultures were positioned over the electrode array in such a way that a proportion of the electrodes was covered with neuronal cell bodies, with
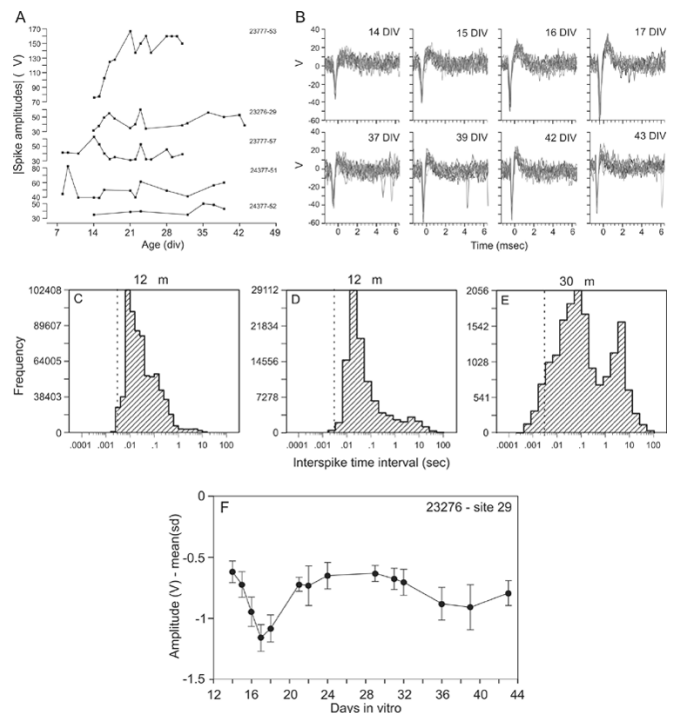

Fig. 4. (a) Display of absolute amplitudes of the negative spikes measured at several time points during entire recording periods in three different experiments at five recording sites (as indicated on the right). (b) Shapes of action potentials, recorded at site 29 in preparation #23276, at several days in the early and the late phase of the recording. Each panel displays the superposition of ten traces, demonstrating the stability of the spike shape throughout the recording period. Also noise levels remain stable at about 7-μV rms (c), (d) Interspike interval distributions calculated from the intervals at (c) site 29 and (d) site 55 during 1 h daily for the whole recording period. The dashed lines at 3 ms indicate the cutoff due to refractory periods. (e). Illustration of an interspike interval distribution from a separate experiment on a HEXA MEA multielectrode array, with the spikes taken from an electrode with a diameter of 30 μm, clearly displaying intervals below the refractory period cutoff, thus indicating spiking activity from more than one unit on this large electrode. (f) Mean (sd) values of spike amplitudes (after amplification) at site 29 in preparation #23 276 during the entire recording period, illustrating overall stability as well as periods of gradual changes in the mean spike amplitudes.

the remainder covered only by the axonal network, have shown that, whereas activity is readily picked up from electrodes contacting cell bodies, no spikes are detectable from electrodes in contact with only the axons.

B. Electrode Size and Firing Rates

Because of the small size of the electrodes (12 μm diameter), each electrode can make contact with a single or only a few neurons at the most. To measure the effect of electrode size on the detected firing rates, experiments were done with multielectrode arrays having electrodes of different diameter (10, 20, and 30 μm—HEXA MEAs from Multichannel Systems). Mean firing rates over three weeks of recording proved to be equal for the 10- and 20-μm electrodes but significantly higher for the 30-μm electrodes (Table I), demonstrating that while the 30-μm electrode has picked up activity from more than one neuron the measured activity from electrodes less than 20 μm in diameter originate from a single unit. The multiunit contribution to 30-μm electrodes is also reflected in the interspike interval distributions, showing intervals smaller than the refractory period of 2-3 ms [Fig. 4(e)].

TABLE I
MEAN FIRING RATES (NUMBER OF SPIKES PER HOUR) OVER A PERIOD OF
THREE WEEKS *IN VITRO* AT ELECTRODES WITH DIFFERENT TIP DIAMETERS

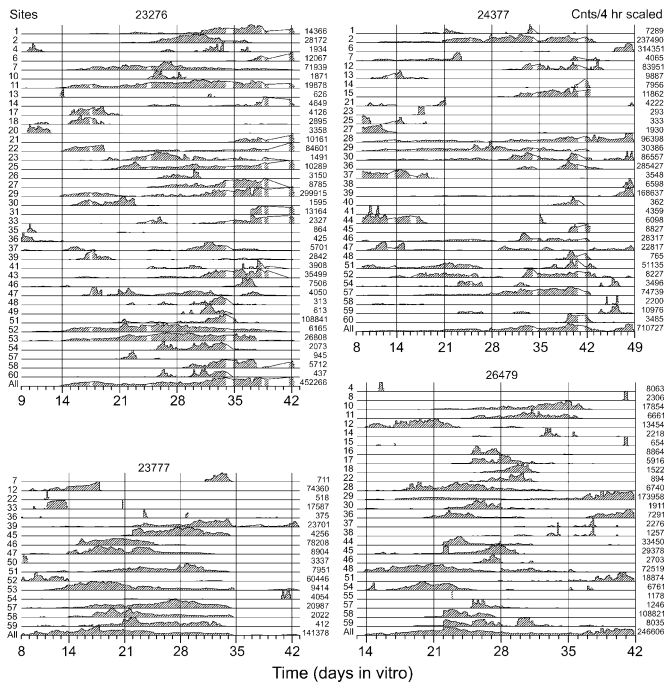| 10 micron Mean (sem)	20 micron Mean (sem)	30 micron Mean (sem)
802 (27)	746 (24)	1410 (39)

Fig. 5. Firing rates expressed as counts per 4-h time bins at the individual sites of the multielectrode array in four preparations for whole periods of recording. The numbers to the left of each panel denote the electrodes, whose locations in the array can be found in Fig. 1(c). The bottom trace shows the summed activity over all sites. Note that the firing rate traces are individually scaled, with the maximum rate per 4-h bin indicated on the right of each panel. In the interest of clarity, only sites with a mean rate exceeding 1 spike/min at some point in time are shown. The plot includes a few interpolated (nonhatched) episodes for which no data were available.

C. Overview and the Time Course of Firing Rates

For each experiment, an overview of the firing rates at all recording sites during the entire period was generated by concatenating all the runs in an experiment and plotting the data as the number of spikes per 4-h bin size per site versus time in culture. In this condensed plot, each site is scaled individually according to the maximum firing rate measured during the whole period of recording (Fig. 5, showing the overview of four of the five experiments, for reasons of space). A remarkable observation from this figure is that individual sites display highly irregular firing rate profiles, with most sites exhibiting one or more periods during which their firing rate is strongly increased. These transient periods last from less than a day up to several weeks and do not appear to be correlated among different sites in the network. Maximum firing rates also differed substantially among the recording sites, as can be seen from the scale numbers to the right of the figure, which range from less than 240 spikes per 4 h (such traces are not displayed here) to almost 300 000 spikes per 4-h time bin from site 29 in preparation
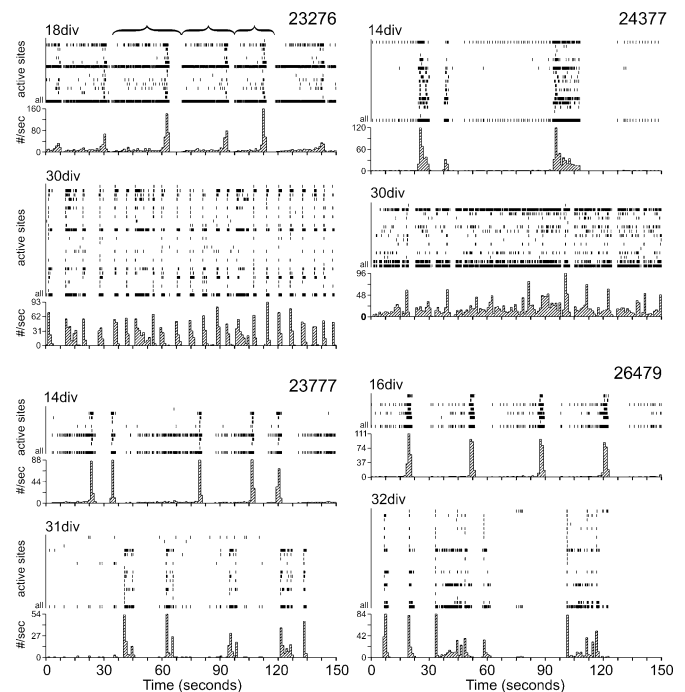

Fig. 6. Spike timings at the individual recording sites and total network firing rates during 150-s time periods. The samples are drawn from four different preparations, at two different developmental time points, i.e., preparation #23 276 at 18 and 30 DIV, prep. #24 377 at 14 and 30 DIV, prep. #23 777 at 14 and 31 DIV, and prep. #26 479 at 16 and 32 DIV. Each panel illustrates the timing of spikes from the individual active sites as well as a trace for the summed activity, indicated by "all." The firing rate trace displays the time course of the total number of network spikes per second. The examples illustrate the repetitive spatio-temporal pattern of network spiking with active and silent phases, the occurrence of network bursts (short episodes of intense and synchronous firing) within the active phases, the differential contribution of individual sites to the active phase of each repetitive period, and the developmental changes of the repetitive spatio-temporal firing patterns (illustrated here for the third and fifth WIV). The three repetitive periods of network firing in preparation #23 276 at 18 DIV, indicated by the horizontal braces, are displayed in more detail in Fig. 7.

#23 276. During the phases of increasing or decreasing firing rates, it was verified that spike signals maintained their amplitudes and waveforms. Summed activity over the entire network, displayed in the bottom traces of Fig. 5, showed only gradual changes in firing rate (apparent on a coarse time scale of several days or weeks).

D. Time Course of Network Spiking

On a time scale of seconds, network activity showed an ongoing repetition of distinctive firing patterns, typically containing short episodes of intensified, synchronous firing at increased number of sites (*network bursts*). This repetitive pattern was observed throughout the entire duration of the experiments, as shown in Fig. 6 for four different preparations (for reasons of space) at two different time points. Each panel in this figure displays both the timing of the individual spikes at all the active recording sites, and the firing rates of total network spiking, in number of spikes per second, during a period of 150 s. The repetitive pattern of network activity is best illustrated by the spike trace of summated network spiking (designated by "all") and by the firing rate plot. For instance, at 18 DIV in preparation #23276, three such repetitions (indicated by horizontal braces) start with a relatively long phase of low
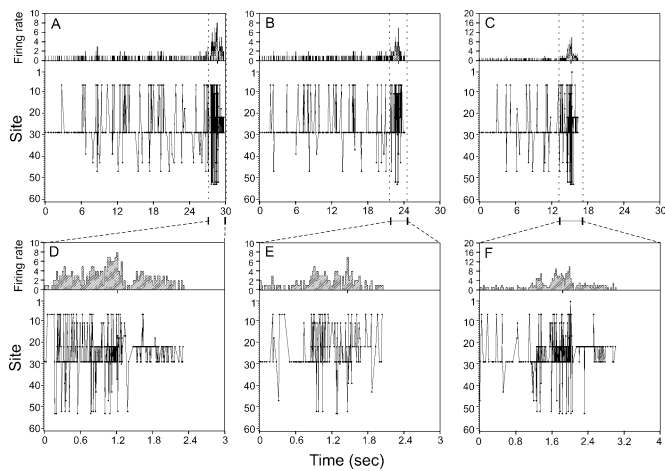
Fig. 7. (a)–(c) Display of three consecutive repetitive periods of network firing extracted from preparation #23 276 at 18 DIV (see Fig. 6, horizontal braces). The top part of each panel displays the total firing rate as the number of spikes per time bin of 25 ms. The bottom part of each panel displays the exact timing of the individual spikes (dots) for each of the sites. Consecutive spikes are connected by thin lines in order to indicate the temporal order of the individual spikes. The dominant firing at site 29 is clearly visible by the sequence of dots for this site. All three repetitive periods show a transient increase of firing rate at their ends (viz. *network bursts*), approximately in the time window bounded by the vertical dashed lines. The bottom row of panels (d)–(f) display an expanded view of the network bursts. In each panel the center of the network burst is indicated by a small line drawn underneath the total firing rate plot. These centers are used as alignment time marks for the summation of consecutive network bursts. Note the complete suppression of activity after each repetitive period (i.e., onset of the quiescent phase).
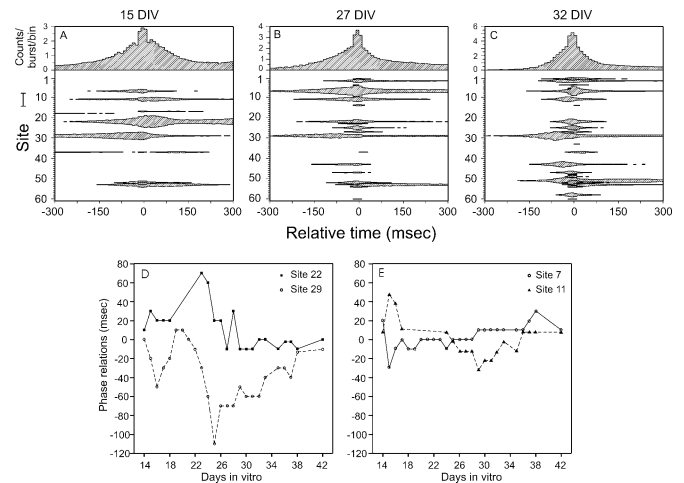

Fig. 8. Total firing rate profile and spatio-temporal organization of network bursts in preparation #23 276 at (a) 15, (b) 27, and (c) 32 DIV. The network burst intensity profiles were obtained by averaging the firing rate during time-aligned individual network bursts detected over consecutive periods of 4 h. Each panel displays (on the upper trace) for a time window of 600 ms, the averaged total network burst intensity as number of spikes per network burst per time bin (10 ms). The lower traces show the average firing rate at individual sites, with the scale bar to the left of the figure indicating a firing rate of one spike per site per network burst per time bin. The bars are plotted symmetrically around their horizontal axes (note, that frequencies smaller than 0.02 spikes per site per network burst per time bin have been omitted from plotting). The figure illustrates how each site contributes to a network burst in a highly specific way, both in amplitude and time point of maximal firing, thus displaying a clearcut temporal order of firing. Panel c also illustrates a drastic shortening of the network bursts after about 4 WIV, while maintaining temporal order among the sites. (d), (e) Time points of peak firing rates at the individual sites relative to the center of the network burst (in units of 10-ms time bins). (d) Site 29 (dashed line) has its peak firing rate earlier than site 22 (continuous line) throughout the whole period of recording. (e) Site 11 (dashed line) and site 7 (continuous line) change temporal order at 25 DIV.

firing rate, followed by a short phase of intense synchronous firing at a larger number of sites (*network burst*), terminated by a short phase of silence. The other experiments show a similar repetitive pattern of network firing around the beginning of the third WIV (Fig. 6).

With time *in vitro*, the repetitive pattern of firing changed progressively, as illustrated in the panels of Fig. 6 for the fifth WIV. These changes are apparent in the frequency of repetition, the firing rate profile, and the contribution of the individual sites. Network bursts also tend to occur during specific phases of each repetition. Whereas network bursts in the third WIV are preceded by a phase of low-level firing, by the fifth WIV they show a much more sudden onset and are frequently followed by a weak after-discharge, as clearly shown in three of the four panels. The 30 DIV pattern of #24 377 is more complex but still includes abrupt onset network bursts. It also appears to be part of a periodic fluctuation of about 5 minutes per cycle, illustrating that also periodicities in firing rates on coarser time scales have been observed.

E. Network Bursts

The three repetitive periods of network firing indicated with horizontal braces in prep. #23 276 at 18 DIV in Fig. 6 are displayed at higher time resolutions in Fig. 7. The traces of the individual sites clearly illustrate the differential contribution of each site to the overall activity, as well as the temporal order of spiking (thin connecting lines). The figures also illustrate how the initial phase of low firing rate is followed by a short phase of increased firing rate with recruitment of hitherto silent sites (*network bursts*). A time-expanded view of these network bursts

is given in panels D-F (Fig. 7), showing in more detail also the tendency of individual sites to fire at a specific phase within the network bursts. For instance, site 29 fires more intensely during network burst onset while site 22 contributes more intensely at the end of the network burst.

These phase relationships become more explicit when consecutive network bursts are summed (see Section II), so that burst-to-burst variations are averaged (Fig. 8).

The firing rate profiles of individual sites during network bursts differ considerably with respect to their shape, peak firing rates, and time of peak firing, thus displaying a clearcut temporal order of firing (Fig. 8). Phase relationships between pairs of sites appear to be highly stable over periods of days, and for many pairs over much longer periods. This has been verified by calculating for each site the time bin of peak firing rate during a network burst and comparing these site centers over the recording period. For instance, site 29 has its peak firing earlier than site 22 in prep. #23 276 as is shown in Fig. 8(a)–(c). Actually, sites 29 and 22 maintain their temporal order from 14 through 42 DIV [Fig. 8(d)]. Inversion of temporal order also occurs, as shown for instance between sites 7 and 11, where site 7 precedes site 11 in peak firing at 15 DIV but by 32 DIV has come to lag behind it Fig. 8(a)–(c), while Fig. 8(e) shows that the order reversal occurs at 25 DIV. Thus, although the firing rate profiles within network bursts are remarkably stable over
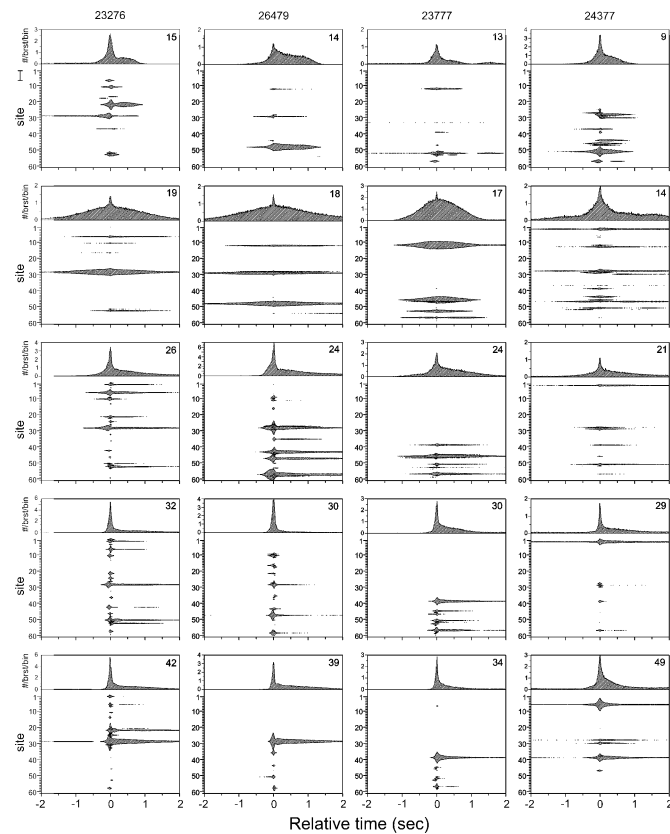
Fig. 9. Total firing rate profile and spatio-temporal organization of network bursts in four preparations, with representative examples at five different developmental stages *in vitro*. The columns illustrate the developmental progression in network burst firing rate profiles in four experiments. For each experiment (column), the time points displayed are selected so as to best illustrate the characteristic differences in network burst intensity profiles. (On a day-to-day basis, the illustrated network burst intensity profiles evolved smoothly into one another.) For an explanation of each panel, see the caption of Fig. 8.
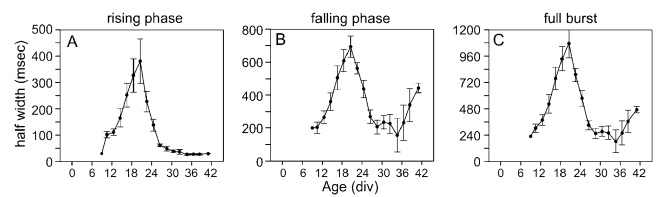

Fig. 10. Half-width of (a) rising phase, (b) falling phase, and (c) full network bursts during network development *in vitro*. Half-width values are calculated from averaged network burst intensity profiles obtained by summation of all network burst encountered on each day. The figure summarizes the mean and SEM values per day for all five longitudinal experiments.

periods of several days, they can change gradually over longer periods of development *in vitro* (Fig. 9).

All five experiments have shown a generally similar developmental progression in these profiles, with an initial broadening of network bursts up to a half-width of about 1 s in the third WIV, followed by a drastic shortening of the rising phase and a strong reduction in the falling phase. By about one month *in vitro*, network bursts have evolved into events with an abrupt onset (with a half width of about 30 ms for the rising phase) and an after-discharge adding up to a total burst half-width between 200 and 500 ms (Fig. 10). This abrupt onset of network burst firing persisted for the remaining period *in vitro*, while the after-discharge showed a moderate lengthening in the seventh WIV. As also shown in Fig. 9, on a day-to-day basis network burst intensity profiles evolved smoothly and progressively into one another.

IV. DISCUSSION

A. Long-Term Recording of Network Firing

The large number of "active sites" (for instance, the sites displayed in Fig. 5, showing peak firing rates of at least 1 spike per minute, represent 28%–65% of the total number of 60 sites) indicates that the density of cortical neurons used in the present experiments, which resulted in a confluent monolayer of cells, enabled adequate electrical contact to be frequently made with the electrodes. Visual inspection of spike shapes and amplitudes on storage oscilloscope traces showed single-unit activity at about 50% of the active sites. In the case of multiunit activity, large spike amplitudes were generally accompanied by smaller spikes such that amplitude discrimination was still effective in selecting a single unit. A single-unit origin for detected spike trains was further supported on the basis of refractory periods of 2–3 ms in the interspike interval histogram. These findings are in fact consistent with what can be expected on the basis of the size of the electrodes and the cell bodies. For a good signal-to-noise ratio, a substantial part of the cell body needs to be in contact with the electrode surface [31], [32]. With de-insulated electrode areas of 12 μm, and cell bodies of about 10 μm in diameter, one can expect either complete coverage or shared coverage by at most, two or three neuronal cell bodies. Shared coverage will hardly ever occur when the electrode is smaller than the cell body but will be more frequent with larger electrode sizes. The probability of measuring spikes from multiple units should depend in a similar way on the electrode size, which expectation was confirmed by data obtained using multielectrode arrays (HEXA MEAs) with different electrode sizes (see Table I). These data showed that a tip diameter increase from 10 to 20 μm failed to result in capturing activity from any additional unit whereas only a still further increase to 30 μm was capable of doing so. Thus, the activity recorded at the smaller electrodes of 10- and 20-μm diameter must indeed be regarded as being of single-unit origin.

The contribution of axonal spikes to the detected firing activity at the electrodes was negligible, which is hardly surprising since individual axons cannot achieve sufficient sealing of an electrode to transmit large enough action potentials to pass threshold setting. This was verified by observations that axons in our cultures do not form bundles but, rather, course through the culture as a loose meshwork which is not dense enough to cover an electrode. Moreover, since axons grow out only after adhesion of the cell bodies, they grow around or over cell bodies but not under them, a fact which was verified in our own cultures by the use of confocal microscopy (data not presented).

B. Long-Lasting Periods of Increased Firing Rates

All experiments showed periods of increased firing rates during network development, lasting for a few days up to several weeks and starting and ending at widely differing times for different recording sites. Peak firing rates, too, differed greatly

among the sites. Given the observed stability in the position of the neurons in the culture, these changes can only originate from fluctuations in the activity levels in the individual neurons, a conclusion further supported by the observed stability among neurons in the temporal relationships of their firing during network bursts. Meandering of a cell over the multielectrode plate would weaken the cell-electrode coupling, resulting in a gradual decrease in spike amplitude [31], [32] but a sudden cessation of detection (only at the point when threshold is no longer reached). The observed changes in firing rates, in contrast, are very slow (at the order of days), while large spike amplitudes are maintained throughout the experiments. Cell death can not be the cause either, since the recording sites in fact continue to fire at low rates during the periods of greatly reduced activity.

According to the calcium hypothesis of Kater [21], differences in activity levels may be expected to affect the morphological development of neurons while, conversely, the observed prolonged periods of elevated firing could themselves in part reflect morphological rearrangements among the neurons. Theoretical model studies of network development based on activity-dependent neurite outgrowth have shown that large fluctuations in firing rates can indeed occur on the time scales of neurite outgrowth, and that maximum firing rates typically differ substantially among functionally identical neurons comprising the network [36]. The developmental profile of total network firing rate, thus, depends on many highly variable components, so that it is hardly surprising that these summed activity profiles from restricted samples vary from one experiment to the next, and fail to show any systematic developmental progression. A similar lack of systematic developmental changes in overall firing levels has previously been reported in single electrode cross-sectional studies using comparable dissociated cortical cell cultures (see [10] and [37]).

C. Repetitive Pattern of Network Firing

The repetitive character of network firing is a prominent feature of network activity in all experiments, which is most clearly demonstrated on a time-scale of seconds. On quite a few occasions, however, periodic fluctuations in firing rate were also observed on coarser time scales, as reported for organotypic neocortical slice cultures as well (e.g., [2]). For instance, the 150-s spiking pattern displayed in Fig. 6 for experiment #24 377 at 30 DIV was actually part of a periodic fluctuation of about 5 min. Although this is a common phenomenon in developing neural tissue (reviewed in [2]), a quantitative analysis of multiscale firing rate periodicities was considered beyond the scope of this paper.

D. Network Bursts

The repetitive occurrence of stereotyped network bursts, invariably observed throughout the entire recording period in all experiments, confirms earlier impressions from organotypic [38] as well as dissociated spinal cord cultures (e.g., [39]). The present study has revealed that these bursts nevertheless change systematically in shape as a function of age *in vitro*, with the most drastic changes in burst intensity profiles taking place during the first 4 WIV. From then on, the burst intensity profiles

are quite stable, in agreement with earlier reports of stabilized activity patterns in neocortical cell cultures only from about 30 DIV [40]. Also in agreement with the present findings, multiple unit recordings from both organotypic cultures [2] and from lightly anesthetized rat neocortex *in vivo* [41], [42] show evolving spontaneous firing patterns throughout the first month of postnatal life.

Previous studies using multielectrode arrays (e.g., [43]–[48]) have reported the appearance of synchronized bursts at around 10 DIV, lasting a few hundred milliseconds and recurring every few seconds. Reference [40] reported burst durations of about 100 and 450 ms after 30 DIV, while [49] described intracellular calcium transients under low Mg^{2+} conditions that were synchronous with bursts of neuronal firing. Our present observations on network burst durations at these time points are in line with these reported values, as well as with studies using more conventional culture techniques (e.g., [5] and [50]). In addition, the present longitudinal studies have revealed a pronounced broadening of network bursts in the third WIV, a phenomenon which has not previously been reported.

An interesting observation was that, in the early weeks of development, the network bursts were preceded by a ramp-like phase of low firing, followed by almost or complete silence, whereas at later stages such bursts had a sudden onset and were often followed by an after-discharge of lower intensity firing (see, for instance, the third and fifth WIV panels in Fig. 6). These findings are reminiscent of observations by [51] at 30 DIV, where early and late phases in the responses of dissociated rat cortical cultures to electrical stimulation could be distinguished. Since spiking during the early response phase (viz. the first 25 ms) occurred with little jitter and precise timing, the neocortical networks in the present study presumably eventually attain a state of excitability such that intrinsic as well as applied stimuli [51] tend to result in the almost instantaneous triggering of a generalized network burst.

By the end of the third WIV, at which time network bursts have attained their maximum duration, the neocortical cell cultures have passed through a period of delayed development of synaptic inhibition relative to excitatory neurotransmission [52] and have reached peak values for the numerical densities of dendritic spine as well as shaft synapses (putatively excitatory and inhibitory, respectively) [53]. These morphological developments could be partly responsible for the parallel physiological changes, since increasing inhibitory feedback has the effect of prolonging the initially short but intense bursts characteristic of very immature networks. Thus, GABAergic disinhibition of 3-week-old cortical cultures, in which network bursts have become longer and less intense, induces the cultures to return to their primitive bursting pattern (see [5] and [10]). The simultaneously increasing density of excitatory (i.e, spine) synapses [53] may be expected to prolong burst durations still more. Conversely, the extreme shortening of network bursts which takes place in the fourth WIV coincides with a "pruning" of dendritic spine, but not shaft, synapses to a much lower plateau level [52], thus shifting the balance of synaptic excitation and inhibition strongly in favor of the latter. The proposition suggests itself that now, in contrast with immature cultures, it will be GABAergic inhibitory feedback rather than intrinsic channel dynamics (see [2]) which is responsible for

terminating each network burst. Indeed, in organotypic cortical explants, the oldest cultures studied showed a clearcut lengthening rather than shortening of each burst upon exposure to GABAergic receptor blocking agents [2]. This putative age-dependent regulation of the duration of network discharges by inhibitory synaptic mechanisms is currently being investigated experimentally in dissociated cell cultures using multielectrode recording techniques.

Removal of excessive excitatory synapses might also contribute to the abrupt onset of network bursts characteristic of mature cell cultures in the present study, in contrast with the ramp-like buildup of spike activity which precedes each burst in the younger cultures. This could be the case if such pruning operates to selectively remove synapses which fail to contribute to an optimal responsiveness to incoming stimuli or to efficient channeling of excitation through the neural network. This is a highly complex process which depends upon a large number of interrelated dynamic factors regulating neuronal excitability [2]. The question of how such optima become established and how they are able to be effectuated by developing cortical networks will, therefore, undoubtedly require the help of computer simulation studies in order to test the plausibility of putative mechanisms. Algorithmic and living cellular "model systems" may, thus, need to actively complement each other in our striving for insights into the functional development of the intact brain.

E. Timing of Neuronal Firing Within Network Bursts

The averaged spatio-temporal structure of network bursts has made it clear that neurons differ not only in their mean firing rate but also in the temporal order of their recruitment within network bursts. Since timing relationships between synaptically connected neurons originate from synaptic delays and electrotonic spread of post-synaptic potentials, the observed temporal relationships must be giving functional indications about the connectivity of neurons within the network. The observed stability of temporal relationships over long periods of network development, starting from the earliest weeks *in vitro*, thus, suggests that parts of the original connectivity structure are highly conserved, a finding which is perhaps unexpected for a network still undergoing pronounced developmental changes. Changes in the temporal order of spiking could be indicative of altered connectivity, causing a rerouting of firing activity through the network. This would make the temporal order structure within network bursts a potentially sensitive measure for the topology of network connectivity. Recently, [54] has also reported highly stable phase relationships in spontaneous firing between pairs of cultured neocortical neurons, albeit only for the duration of 5-h recording periods.

A number of recent studies have demonstrated a critical role for spike timing in activity-dependent synaptic plasticity. For instance, [55] found synaptic strengthening or weakening when presynaptic action potentials precede or follow, respectively, postsynaptic spikes within critical windows of not more than 20 ms. Assuming that similar mechanisms are operative in cortex tissue cultures (e.g., [27] and [56]), the repetitive occurrence of network bursts (with a synchronized onset of less than 100 ms in mature cultures) would provide favorable conditions for spontaneously effectuating activity-dependent synaptic plasticity rules. Recent model studies have shown that a spike-timing-dependent plasticity rule indeed can selectively promote inputs that elicit postsynaptic firing at short latencies [57]. The observed shortening of network bursts with age in the present report also implies a reduction in the upper limit of firing latencies between neurons contributing to the burst. Whether this increased precision of spike timing, along with the abrupt onset of network bursts at later developmental stages is the result of refinement of synaptic connectivity under the influence of previous network activity is an intriguing question which may well be approachable using long-term spatio-temporal monitoring in appropriately simplified "model" systems such as the one employed in the present study.

In summary, the present longitudinal recordings of firing activity within developing neocortical networks have brought to light several developmental changes in network dynamics, reproducibly observed in several independent experiments. These include observations of: 1) uncorrelated transients of increased firing rates at individual sites, lasting for days up to weeks; 2) a repetitive pattern of network spiking on a time scale of seconds; 3) repetitive occurrences of synchronized network bursts showing highly stable spatio-temporal firing profiles over time periods of many hours, but with progressive slow changes over periods of days; 4) a pronounced broadening of network bursts up to a half-width of about 1 s in the third WIV, followed by a drastic shortening toward a profile with a rising phase half-width of about 30 ms, with greatly increased precision of spike timing; and 5) an overall stability throughout development in the temporal order of spiking among individual sites during network bursts.

REFERENCES

[1] M. A. Corner, "Spontaneous motor rhythms in early life—Phenomenological and physiological aspects," *Prog. Brain Res.*, vol. 48, pp. 349–364, 1978.

[2] M. A. Corner, J. van Pelt, P. S. Wolters, R. E. Baker, and R. Nuytinck, "Physiological effects of sustained blockade of excitatory synaptic transmission on spontaneously active developing neuronal networks—An inquiry into the reciprocal linkage between intrinsic biorhythms and neuroplasticity in early ontogeny," *Neurosci. Biobehav. Rev.*, vol. 26, pp. 127–185, 2002.

[3] M. B. Feller, "Spontaneous correlated activity in developing neural circuits," *Neuron*, vol. 22, pp. 653–656, 1999.

[4] M. J. O'Donovan, "The origin of spontaneous activity in developing networks of the vertebrate nervous system," *Curr. Opin. Neurobiol.*, vol. 9, pp. 94–104, 1999.

[5] M. A. Corner and G. J. A. Ramakers, "Spontaneous firing as an epigenetic factor in brain development—Physiological consequences of chronic tetrodotoxin and picrotoxin exposure in cultured rat neocortex neurons," *Dev. Brain Res.*, vol. 65, pp. 57–64, 1992.

[6] R. D. Fields and P. G. Nelson, "Activity-dependent development of the vertebrate nervous system," *Int. Rev. Neurobiol.*, vol. 34, pp. 133–214, 1991.

[7] C. S. Goodman and C. J. Shatz, "Developmental mechanisms that generate precise patterns of neuronal connectivity," *Cell*, vol. 72, pp. 77–98, 1993.

[8] J. van Pelt, A. van Ooyen, and M. A. Corner, "Growth cone dynamics and activity-dependent processes in neuronal network development," *Prog. Brain Res.*, vol. 108, pp. 333–346, 1996.

[9] M. C. Crair, "Neuronal activity during development: Permissive or instructive?," *Curr. Opin. Neurobiol.*, vol. 9, pp. 88–93, 1999.

[10] G. J. A. Ramakers, M. A. Corner, and A. M. M. C. Habets, "Development in the absence of spontaneous bioelectric activity results in increased stereotyped burst firing in cultures of dissociated cerebral cortex," *Exp. Brain Res.*, vol. 79, pp. 157–166, 1990.

[11] N. C. Spitzer, "Spontaneous activity: Functions of calcium transients in neuronal differentiation," *Persp. Dev. Neurobiol.*, vol. 2, pp. 379–386, 1995.

[12] ——, "New dimensions of neuronal plasticity," *Nature Neurosci.*, vol. 2, pp. 489–491, 1999.

[13] ——, "A developmental handshake: Neuronal control of ionic currents and their control of neuronal differentiation," *J. Neurobiol.*, vol. 22, pp. 659–673, 1991.

[14] M. A. Corner, "Reciprocity of structure-function relations in developing neural networks," *Prog. Brain Res.*, vol. 102, pp. 3–31, 1994.

[15] A. van Ooyen, "Activity-dependent neural network development," *Network: Comput. Neural Syst.*, vol. 5, pp. 401–423, 1994.

[16] M. S. Marom and G. Shahaf, "Development, learning and memory in large random networks: Lessons beyond anatomy," *Qu Rev. Biophys.*, vol. 35, pp. 63–87, 2002.

[17] R. D. Fields, E. A. Neale, and P. G. Nelson, "Effects of patterned electrical activity on neurite outgrowth from mouse sensory neurons," *J. Neurosci.*, vol. 10, pp. 2950–2964, 1990.

[18] G. J. A. Ramakers, J. Winter, T. M. Hoogland, M. B. Lequin, J. van Pelt, and C. W. Pool, "Depolarization stimulates lamellipodia formation and axonal, but not dendritic branching in cultured rat cerebral cortex neurons," *Dev. Brain Res.*, vol. 108, pp. 205–216, 1998.

[19] R. E. Baker, P. Wolters, and J. van Pelt, "Chronic blockade of glutamate-mediated bioelectric activity in long-term organotypic neocortical explants differentially effects pyramidal/nonpyramidal dendritic morphology," *Dev. Brain Res.*, vol. 104, pp. 31–39, 1997.

[20] S. B. Kater, M. Mattson, C. S. Cohan, and J. Connor, "Calcium regulation of the neuronal growth cone," *Trends Neurosci.*, vol. 11, pp. 315–321, 1988.

[21] S. B. Kater, R. W. Davenport, and P. B. Guthrie, "Filopodia as detectors of environmental cues: Signal integration through changes in growth cone calcium levels," *Prog. Brain Res.*, vol. 102, pp. 49–60, 1994.

[22] G. J. A. Ramakers, F. C. Raadsheer, M. A. Corner, F. C. S. Ramaekers, and F. W. van Leeuwen, "Development of neurons and glial cells in cerebral cortex, cultured in the presence or absence of bioelectric activity: Morphological observations," *Eur. J. Neurosci.*, vol. 3, pp. 140–153, 1991.

[23] J. van Pelt, P. S. Wolters, W. L. C. Rutten, M. A. Corner, P. van Hulten, and G. J. A. Ramakers, "Spatio-temporal firing in growing networks cultured on multi-electrode arrays," in *Proc. World Congr. Neuroinformatics*, F. Rattay, Ed., 2001, Argesim Report no. 21, pp. 462–467.

[24] G. W. Gross, "Simultaneous single unit recording *in vitro* with a photo-etched laser de-insulated gold multi-electrode surface," *IEEE Trans. Biomed. Eng.*, vol. BME-26, pp. 273–278, 1979.

[25] G. W. Gross and F. U. Schwalm, "A closed flow chamber for long-term multichannel recording and optical monitoring," *J. Neurosci. Meth.*, vol. 52, pp. 73–85, 1994.

[26] J. Pine, "Recording action potentials from cultured neurons with extracellular microcircuit electrodes," *J. Neurosci. Meth.*, vol. 2, pp. 19–31, 1980.

[27] Y. Jimbo, T. Tateno, and H. P. C. Robinson, "Simultaneous induction of pathway-specific potentiation and depression in networks of cortical neurons," *Biophys. J.*, vol. 76, pp. 670–678, 1999.

[28] W. L. C. Rutten, J. M. Mouveroux, J. Buitenweg, C. Heida, T. Ruardi, E. Marani, and E. Lakke, "Neuro-electronic interfacing with cultured multi-electrode arrays toward a cultured probe," *Proc. IEEE*, vol. 89, pp. 1013–1028, July 2001.

[29] M. Meister, J. Pine, and D. A. Baylor, "Multi-neuronal signals from the retina: Acquisition and analysis," *J. Neurosci. Meth.*, vol. 51, pp. 95–106, 1994.

[30] G. W. Gross, W. Y. Wen, and J. W. Lin, "Transparent indium-tin oxide electrode patterns for extra-cellular, multi-site recording in neuronal cultures," *J. Neurosci. Meth.*, vol. 15, pp. 243–252, 1985.

[31] J. R. Buitenweg, W. L. C. Rutten, W. P. A. Willems, and J. W. van Nieuwkasteele, "Measurement of sealing resistance of cell-electrode interfaces in neuronal cultures using impedance spectroscopy," *Med. Biol. Eng. Comp.*, vol. 36, pp. 630–637, 1998.

[32] W. G. Regehr, J. Pine, C. S. Cohan, M. D. Mischke, and D. W. Tank, "Sealing cultured invertebrate neurons to embedded dish electrodes facilitates long-term stimulation and recording," *J. Neurosci. Meth.*, vol. 30, pp. 91–106, 1989.

[33] S. M. Potter and T. B. Demarse, "A new approach to neural cell culture for long-term studies," *J. Neurosci. Meth.*, vol. 110, pp. 17–24, 2001.

[34] J. H. Cocatre-Zilgien and F. Delcomyn, "Identification of bursts in spike trains," *J. Neurosci. Meth.*, vol. 41, pp. 19–30, 1992.

[35] J. R. Buitenweg, W. L. Rutten, and E. Marani, "Modeled channel distributions explain extracellular recordings from culture neurons sealed to microelectrodes," *IEEE Trans Biomed Eng.*, vol. 49, pp. 1580–90, Dec. 2002.

[36] A. van Ooyen and J. van Pelt, "Complex periodic behavior in a neural network model with activity-dependent neurite outgrowth," *J. Theor. Biol.*, vol. 179, pp. 229–242, 1996.

[37] A. M. M. C. Habets, A. van Dongen, F. van Huizen, and M. A. Corner, "Spontaneous neuronal firing patterns in fetal cortical networks during development *in vitro*," *Exp. Brain Res.*, vol. 69, pp. 43–52, 1987.

[38] S. M. Crain, *Neurophysiologic Studies in Tissue Culture*. New York: Raven Press, 1976.

[39] M. H. Droge, G. W. Gross, M. H. Hightower, and L. E. Czisny, "Multielectrode analysis of coordinated, multisite, rhythmic bursting in cultured CNS monolayer networks," *J. Neurosci.*, vol. 6, pp. 1583–1592, 1986.

[40] H. Kamioka, E. Maeda, Y. Jimbo, H. P. C. Robinson, and A. Kawana, "Spontaneous periodic synchronized bursting during formation of mature patterns of connections in cortical cultures," *Neurosci. Lett.*, vol. 206, pp. 109–112, 1996.

[41] M. A. Corner and M. Mirmiran, "Spontaneous neuronal firing patterns in the occipital cortex of developing rats," *Int. J. Devel. Neurosci.*, vol. 8, pp. 309–316, 1990.

[42] M. A. Corner, C. G. van Eden, and A. J. de Beaufort, "Spike-train analysis reveals "Overshoot" in developing rat prefrontal cortex function," *Brain Res. Bull.*, vol. 28, pp. 799–802, 1992.

[43] E. Maeda, H. P. C. Robinson, and A. Kawana, "The mechanisms of generation and propagation of synchronized bursting in developing networks of cortical neurons," *J. Neurosci.*, vol. 15, pp. 6834–6845, 1995.

[44] Y. Jimbo and H. P. C. Robinson, "Propagation of spontaneous synchronized activity in cortical slice cultures recorded by planar electrode arrays," *Bioelectrochem.*, vol. 51, pp. 107–115, 2000.

[45] P. E. Latham, B. J. Richmond, S. Nirenberg, and P. G. Nelson, "Intrinsic dynamics in neuronal networks. II. experiment," *J. Neurophysiol.*, vol. 83, pp. 828–835, 2000.

[46] J. Streit, A. Tscherter, M. O. Heuschkel, and P. Renaud, "The generation of rhythmic activity in dissociated cultures of rat spinal cord," *Eur. J. Neurosci.*, vol. 14, pp. 191–202, 2001.

[47] A. Tscherter, M. O. Herschkel, P. Renaud, and J. Streit, "Spatio-temporal characterization of rhythmic activity in rat spinal cord slice cultures," *Eur. J. Neurosci.*, vol. 14, pp. 179–190, 2001.

[48] R. Segev, Y. Shapira, M. Benvenisto, and E. Ben-Jacob, "Observations and modeling of synchronized bursting in two-dimensional neural networks," *Phys. Rev. E*, vol. 64, 011 920, pp. 1–9, 2001.

[49] Y. Jimbo, H. P. C. Robinson, and A. Kawana, "Simultaneous measurement of intracellular calcium and electrical activity from patterned neural networks in culture," *IEEE Trans. Biomed. Eng.*, vol. 40, pp. 804–810, Aug. 1993.

[50] M. A. Corner and S. M. Crain, "Patterns of spontaneous bioelectric activity during maturation in cultures of fetal rodent medulla and spinal cord tissues," *J. Neurobiol.*, vol. 3, pp. 25–45, 1972.

[51] Y. Jimbo, A. Kawana, P. Parodi, and V. Torre, "The dynamics of a neuronal culture of dissociated cortical neurons of neonatal rats," *Biol. Cybern.*, vol. 83, pp. 1–20, 2000.

[52] G. J. A. Ramakers, H. van Galen, M. G. P. Feenstra, M. A. Corner, and G. J. Boer, "Activity-dependent plasticity of inhibitory and excitatory amino acid transmitter systems in cultured rat cerebral cortex," *Int. J. Devel. Neurosci*, vol. 12, pp. 611–621, 1994.

[53] F. van Huizen, H. J. Romijn, and A. M. M. C. Habets, "Synaptogenesis in rat cerebral cortex is affected during chonic blockade of spontaneous bioelectric activity by tetrodotoxin," *Dev. Brain Res.*, vol. 19, pp. 67–80, 1985.

[54] G. Shahaf and S. Marom, "Learning in networks of cortical neurons," *J. Neurosci.*, vol. 15, pp. 8782–8788, 2002.

[55] L. I. Zhang, W. T. Huizhong, C. E. Holt, W. A. Harris, and M.-M. Poo, "A critical window for cooperation and competition among developing retinotectal synapses," *Nature*, vol. 395, pp. 37–44, 1998.
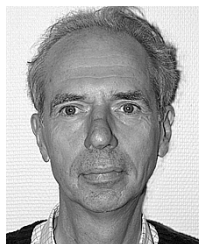
[56] G. Q. Bi and M.-M. Poo, "Synaptic modification by correlated activity: Hebb's postulate revisited," *Annu. Rev. Neurosci.*, vol. 24, pp. 139–166, 2001.

[57] S. Song, K. D. Miller, and L. F. Abbott, "Competitive hebbian learning through spike-timing dependent synaptic plasticity," *Nature Neurosci.*, vol. 3, pp. 919–926, 2000.

Michael A. Corner was born in New York, NY, on April 10, 1933. He received the B.S. degree from the City College of New York, New York, in 1954 and the Ph.D. degree in zoology from Columbia University, New York, in 1962.

Prior to completing his doctoral work, he held positions at Columbia University's College of Physicians and Surgeons, New York, and the Rockefeller Institute for Medical Research, New York. He went to Amsterdam, The Netherlands in 1963, on a postdoctoral fellowship to pursue research in electrophysiology of the developing brain at the Netherlands (Central) Institute for Brain Research, where he still remains active. He is also a Professor (*Emeritus*) of Developmental Physiology at the University of Amsterdam, Amsterdam.

Jaap van Pelt was born in Amsterdam, The Netherlands, on June 14, 1946. He received the M.S. degree in physics and mathematics and the Ph.D. degree in experimental nuclear physics from the Free University of Amsterdam, Amsterdam, The Netherlands, in 1972 and 1978, respectively.

From 1972 to 1974, he fulfilled his military duties with the Royal Dutch Airforce. He joined the Netherlands Institute for Brain Research in 1978 and was engaged in the automation of experimental facilities. In 1983, he became head of the Computer Department and initiated research in computational neuroscience. In 1991, he became the head of the research group Neurons & Networks and initiated an integrated experimental and computational research program on structure-function relations in neurons and neuronal networks.

Wim L. C. Rutten (M'96) received the Ph.D. degree in experimental physics from Leiden University, Leiden, The Netherlands, in 1979.

Thereafter, he studied auditory system with the ENT Department, Leiden University Medical Center. Since 1985, he has been with the Institute for Biomedical Technology (BMTI), Faculty of Electrical Engineering, University of Twente, Enschede, The Netherlands, currently as a Professor of neurotechnology. He is the leader of the Neural and Cellular Engineering program of BMTI/Electrical Engineering. His present research interests are neurotechnology (neuro-electronic interfaces, cultured probe), live learning neural networks, signal processing, and bioelectricity.

Ger J. A. Ramakers was born in Geleen, The Netherlands, on December 10, 1958. He received the B.S. degree in psychology and the M.S. degree in biology from the University of Utrecht, Utrecht, The Netherlands, in 1984 and 1985, respectively, and the Ph.D. degree in biology from the University of Amsterdam, Amsterdam, The Netherlands, in 1991.

From 1991 to 1993, he was a Research Associate with the Molecular Biology and Virology Laboratories, Salk Institute, San Diego, CA. From 1993 to 1995, he was a Research Associate with the Division of Cellular Biochemistry, Netherlands Cancer Institute, Amsterdam. In 1995, he joined The Netherlands Institute for Brain Research, Amsterdam. His interests focus on the structural and functional network determinants of mental retardation and cognition, and the underlying genetic, molecular, and cell biological mechanisms.

Pieter S. Wolters was born in Naarden, The Netherlands, on January 2, 1948. He received the Ing. Engineering degree in electronics from the Rens & Rens School for Electronic Engineering, Hilversum, The Netherlands, in 1972.

In 1975, he joined the Netherlands Institute for Brain Research, Amsterdam, The Netherlands, as a Technician to support research in electron microscopy and electrophysiology.